

SUPPRESSION OF H₂ COOLING IN THE ULTRAVIOLET BACKGROUNDJOHN H. WISE^{1,2} AND TOM ABEL¹*Draft version February 1, 2008*

ABSTRACT

The first luminous objects in the concordance cosmology form by molecular hydrogen cooling in dark matter dominated halos of masses $\sim 10^6 M_\odot$. We use Eulerian adaptive mesh refinement simulations to demonstrate that in the presence of a large soft ultraviolet radiation background, molecular hydrogen is the dominant coolant. Even for very large radiation backgrounds, the halo masses that cool and collapse are up to two orders of magnitude smaller than the halos that cool via atomic hydrogen line cooling. The abundance of cooling halos and the cosmic mass fraction contained within them depends exponentially on this critical mass scale. Consequently, the majority of current models of cosmological reionization, chemical evolution, supermassive black hole formation, and galaxy formation underestimate the number of star forming progenitors of a given system by orders of magnitude. At the highest redshifts, this disagreement is largest. We also show that even in the absence of residual electrons, collisional ionization in central shocks create a sufficient amount of electrons to form molecular hydrogen and cool the gas in halos of virial temperatures far below the atomic cooling limit.

Subject headings: Cosmology: high-redshift — galaxy formation — star formation

1. MOTIVATION

Cosmic structure forms hierarchically. Any object in the universe today, started with copious numbers of small progenitors at redshifts currently inaccessible to direct observations. Traditionally in galaxy formation (Rees & Ostriker 1977; White & Rees 1978; Dekel & Rees 1987; White & Frenk 1991; Baugh et al. 2003) $T_{\text{vir}} = 10^4$ K halos are assumed to be the first cooling halos. Nevertheless since the late 1960's it has been known that molecular hydrogen, formed in the gas phase, can dominate cooling in objects of smaller virial temperature and mass (Saslaw & Zipoy 1967; Peebles & Dicke 1968; Yoneyama 1972; Haiman et al. 1996; Tegmark et al. 1997; Abel et al. 1998, 2000). Neglecting this early phase of H₂ cooling halos has been justified by arguing that H₂ is destroyed via radiative feedback effects (cf. Dekel & Rees 1987; Haiman & Loeb 1997; Haiman et al. 2000; Glover & Brand 2001; Bromm & Loeb 2003). The photo-dissociation of H₂ via the Solomon process by an early soft ultraviolet background (UVB) is generally assumed as the main reason (Oh & Haiman 2002; Ciardi & Ferrara 2005; Haiman & Bryan 2006).

The mass scale of halos considered enters exponentially in the collapsed mass fraction and the abundance of halos. Figure 1 shows the predicted abundances of the earliest building blocks of galaxy formation as a function of redshift for the latest concordance cosmology using the Sheth-Tormen formalism (Press & Schechter 1974; Sheth & Tormen 2002). The different lines correspond to different virial masses. The solid line corresponds to halos with virial temperatures of 10^4 K, the temperature at and above which atomic hydrogen line cooling is domi-

nant. At redshift 30, e.g., the difference of abundances of $2 \times 10^5 M_\odot$ and $T_{\text{vir}} = 10^4$ K halos is five orders of magnitude. Even at redshift 10 this disparity is still a factor of a thousand. When studying reionization and chemical evolution of galaxies and the intergalactic medium, one needs to consider stellar feedback. The simple fact that the binding energy of the gas of smaller mass halos is even less than the kinetic energy deposited by even one supernova (SN) is illustrated in Figure 1B. Surely whether the atomic hydrogen line (Ly α) cooling halos are formed from pristine primordial gas or are mergers of many tens of progenitors that massive stars have enriched and expelled the gas from should make a significant change in their further evolution. The minimum mass of star forming halos is undoubtedly an important issue independent of the techniques employed to study structure formation.

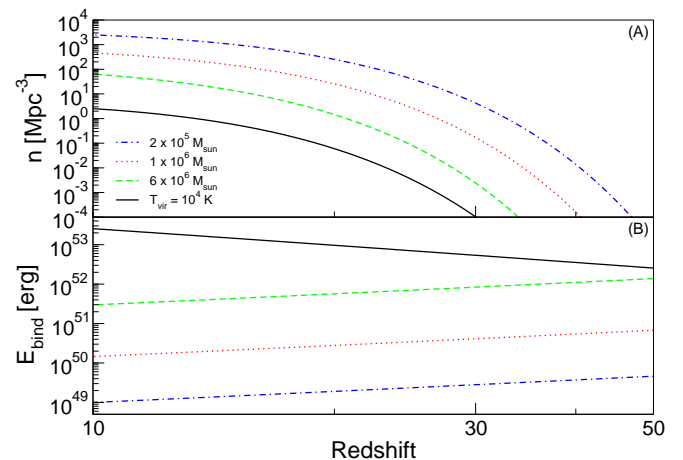


FIG. 1.— *Panel A:* Sheth Tormen number density of dark matter halos as a function of redshift for $T_{\text{vir}} = 10^4$ K, $M = 2 \times 10^5, 10^6$, and $6 \times 10^6 M_\odot$ using WMAP 3 year data for parameters. *Panel B:* Binding energies as a function of redshift for the corresponding halos (same line styles as in panel A)

Electronic address: jwise, tabel@slac.stanford.edu

¹ Kavli Institute for Particle Astrophysics and Cosmology, Stanford University, 2575 Sand Hill Road, MS 29, Menlo Park, CA 94025

² Laboratory for Observational Cosmology, NASA Goddard Space Flight Center, Greenbelt, MD 20771

Advances in cosmological hydrodynamics and its numerical methods (Cen 1992; Zhang et al. 1995; Katz & Hernquist 1996; Abel et al. 1997; Anninos et al. 1997; Bryan & Norman 1998; Gnedin & Abel 2001; Ricotti et al. 2002a,b) allow now detailed investigations of all the relevant physical processes. Modeling the expected negative feedback from an early soft UVB is straightforward as a background flux only causes a spatially constant photo-dissociation rate in the chemical reaction network being solved when H_2 does not exist at high enough abundances to self-shield. Machacek et al. (2001, MBA01 hereafter) used Eulerian adaptive mesh refinement (AMR) simulations to investigate the role of such a H_2 dissociating (Lyman-Werner; LW) background on the minimum mass of halos within which primordial gas can first cool for a variety of radiation amplitudes. In addition to a LW background, the collapse of halos within relic H II regions can be either delayed or catalyzed. Mesinger et al. (2006) used AMR simulations with a short-lived 3 Myr hydrogen ionizing UVB that simulates a nearby massive, metal-free (Pop III) star. They found that halo collapses are prolonged if $J_{21}^{912} \gtrsim 0.1$ and catalyzed if below this critical value, where J_{21}^{912} is in units of $10^{-21} \text{ erg s}^{-1} \text{ cm}^{-2} \text{ Hz}^{-1} \text{ sr}^{-1}$ at a wavelength of 912Å. In the case of a large UVB, the collapse is delayed due to lower gas densities and higher cooling times. In the small UVB regime, excess free electrons in the relic H II region accelerate H_2 formation. In both cases, feedback in relic H II subsides after $\sim 30\%$ of a Hubble time. Strong suppression of H_2 formation also occurs in $10^6 M_\odot$ halos with a LW background $J_{21}^{LW} > 0.01$. Yoshida et al. (2003, YAHS03 hereafter) similarly addressed this issue using smoothed particle hydrodynamics (SPH). They found an additional effect on the minimum collapse mass of dynamical heating from the mass accretion history of the halo. As the heat input increases, the virial temperature must rise before H_2 cooling can start to dominate, and a cool phase develops in the center of the potential well.

Self-consistent calculations in which the sources produce the radiation backgrounds which in turn affect the number of new sources are feasible so far only with semi-analytic approaches (Haiman et al. 2000; Wise & Abel 2005, WA05 hereafter) and small volume cosmological simulations at low spatial resolutions (Ricotti et al. 2002a,b). From these studies, one can derive realistic upper limits on the amplitude of the expected soft UVB. In all studies that include radiation sources in halos less than $10^4 K$ halos, the largest the soft UVB flux can get before the $T > 10^4 K$ halos dominate the emission is $J_{21}^{LW} \sim 1$ (cf. Haiman et al. 2000; Ricotti et al. 2002a,b, WA05). Interestingly, for a LW intensity of $J_{21}^{LW} \sim 0.1$, MBA01 found that $2 \times 10^6 M_\odot$ halos were still able to cool and collapse. On the other hand at that J_{21}^{LW} , YAHS03 suggest negative feedback should become so strong that the critical H_2 fraction for cooling cannot be reached and cooling will not occur. However, they did not explore this further with detailed higher resolution simulations to check whether their analytical expectation would hold.

We present a series of fourteen very high resolution Eulerian AMR simulations designed to see how the largest possible feedback may raise the minimum mass in which primordial gas will cool by molecular hydrogen. The sim-

TABLE 1
SIMULATION PROPERTIES

| Name | H_2 | Residual e^- | F_{LW} | z_a | z_b |
|--------------|-------|----------------|------------|-------|-------|
| H2 | Yes | Yes | 0 | 29.7 | 31.1 |
| H2LW22 | Yes | Yes | 10^{-22} | 28.3 | 27.5 |
| H2LW21 | Yes | Yes | 10^{-21} | 24.4 | 24.7 |
| H2LW20 | Yes | Yes | 10^{-20} | 20.5 | 22.4 |
| noe-H2 | Yes | No | 0 | 18.7 | 23.4 |
| noe-H2LW20 | Yes | No | 10^{-20} | 16.8 | 21.4 |
| H+He | No | Yes | 0 | 15.9 | 16.8 |

NOTE. — These simulations are performed for both realizations.

ulations techniques and details of the suite of calculations is the topic of the next section. In the following sections, we describe the results that show H_2 cooling cannot be neglected in early structure formation. In the discussion, we describe the nature of the UVB and why H_2 cooling can occur in such large radiation backgrounds. We also comment on the large range of questions in cosmological structure formation that this conclusion affects.

2. SIMULATIONS AND ASSUMPTIONS

We use the Eulerian AMR hydrodynamic code *Enzo* (Bryan & Norman 1997, 1999) to study the importance of H_2 cooling in early galaxy formation. *Enzo* uses an n -body adaptive particle-mesh solver (Couchman 1991) to follow the dark matter (DM) dynamics. We perform two cosmological realizations with different box sizes and random phases and WMAP 1 year parameters of $(h, \Omega_\Lambda, \Omega_M, \Omega_b, \sigma_8, n) = (0.72, 0.73, 0.27, 0.024h^{-2}, 0.9, 1)$ (Spergel et al. 2003). The significantly different third year WMAP (WMAP3; Spergel et al. 2007) results favor lesser small-scale power that delays high-redshift structure formation by $\sim 40\%$ and alters the statistical properties of DM halos (Alvarez et al. 2006b). The ratio Ω_M/Ω_b also only lowered by 5% to 5.70. However these differences have no effect on the evolution and assembly of individual halos studied here that have typical mass accretion histories.

The initial conditions are the same as in Wise & Abel (2007). Both realizations have a top grid with a resolution of 128^3 with three nested subgrids with twice finer resolution and are initialized at $z = 129$ (119)[‡] with the COSMICS package (Bertschinger 1995, 2001). The box size is 1.0 (1.5) comoving Mpc. The innermost grid has an effective resolution of 1024^3 with DM particle masses of 30 (101) M_\odot and a side length of 250 (300) comoving kpc. We refine the AMR grids when either the DM (gas) exceeds three times the mean DM (gas) density on the same level. We also refine so that the local Jeans length is resolved by at least 4 cells.

We focus on the region containing the most massive halo in the simulation box and follow its evolution until it collapses to an overdensity of 10^7 that corresponds to a refinement level of 15 and a spatial resolution of ~ 3000 (4000) proper AU.

We perform each realization with seven sets of assumptions. Table 1 summarizes them. We use a nine-species (H, H^+ , He, He^+ , He^{++} , e^- , H_2 , H_2^+ , H^-) non-equilibrium chemistry model (Abel et al. 1997;

[‡] To simplify the discussion, simulation A will always be quoted first with the value from simulation B in parentheses.

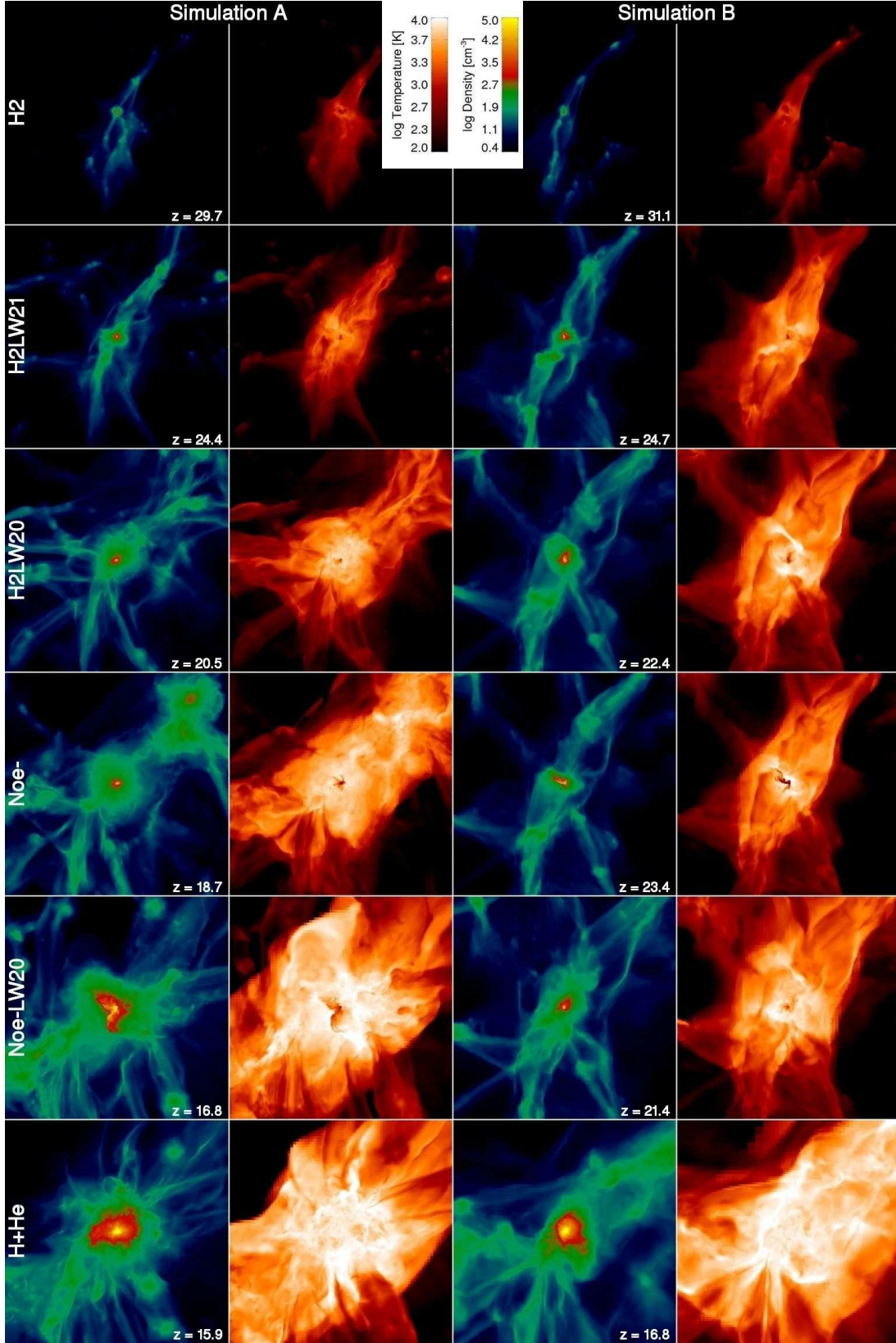


FIG. 2.— Density-squared weighted projections in simulation A (left two columns) and B (right two columns) of the gas density (first and third columns) and temperature (second and fourth columns) at the times when the most massive halo starts to cool and collapse above an overdensity of 10^7 in the models. The rows show the H₂, H2LW21, H2LW20, and noe-H₂, noe-H2LW20, and H+He runs from top to bottom, respectively. Note the complex structure for the SimA-Noe-LW20 and SimB-Noe-H₂ run in which central shocks lead to the formation of free electrons that promote the formation of H₂ and triggering the collapse. The field of view in all panels is 1.2 proper kpc. The color maps are equal for all images.

Anninos et al. 1997) for all runs except the H+He runs that do not include H_2 cooling. The nine-species runs are specified by “H2” and use the H_2 cooling rates from Galli & Palla (1998). Above number densities of 10^4 cm^{-3} or in an intense ultraviolet radiation field, the excited states of H_2 become populated. The H_2 collisional dissociation rates from Abel et al. (1997) are calculated in the ground state; therefore we use a density dependent H_2 dissociation rate from Martin et al. (1996) that considers this phenomenon. Runs with H_2 dissociating (Lyman-Werner; LW) radiation are denoted by “LW” followed by its negative log-flux. We set F_{LW} to 10^{-22} , 10^{-21} , and $10^{-20} \text{ erg s}^{-1} \text{ cm}^{-2} \text{ Hz}^{-1}$ because the first two are typical values one finds in semi-analytic models of reionization and the latter investigates the case of an very large UVB (e.g. Haiman et al. 2000; Wise & Abel 2005). We use the H_2 photo-dissociation rate coefficient for the Solomon process from Abel et al. (1997) of $k_{\text{diss}} = 1.1 \times 10^8 F_{LW} \text{ s}^{-1}$. We do not consider the self-shielding of LW photons. Because the molecular core only becomes optically thick in the late stages of collapse and above column densities of 10^{14} cm^{-2} (Draine & Bertoldi 1996), we expect our results to not be drastically affected by neglecting LW self-shielding. Additionally, LW self-shielding may be unimportant up to column densities of $10^{20} - 10^{21} \text{ cm}^{-2}$ if the medium contains very large velocity gradients and anisotropies (Glover & Brand 2001).

Free electrons are necessary to form H_2 in the gas phase. In order to restrict H_2 formation to $\text{Ly}\alpha$ line cooling halos in our “noe-” calculations, we reduce the residual free electron fraction from $\sim 10^{-4}$ (Peebles 1968; Shapiro et al. 1994) to a physically low 10^{-12} at the initial redshift. This setup is designed to find the first halos that can collapse and form stars once free electrons from collisionally ionized hydrogen becomes available to catalyze H_2 formation (Shapiro & Kang 1987).

This work is an extension of the original work of MBA01, adding the calculations with $F_{LW} = 10^{-20}$ and ones in which H_2 cannot cool until $\text{Ly}\alpha$ cooling becomes efficient. We consider these extreme cases to strengthen the point made in MBA01 in which a UVB only increases the critical halo collapse mass, never completely suppressing the crucial importance of H_2 formation and cooling. Our maximum spatial resolution in the finest AMR level is a factor of four smaller than MBA01; however, this does not cause any differences between our work and MBA01 because these finest grid patches only exist in the dense, central core during the final 150 kyr of the collapse.

2.1. Virial Temperature

In galaxy formation models, the virial temperature is a key quantity as it controls the cooling and star formation rates in a given halo. We define a halo as the material contained in a sphere of radius r_{200} enclosing an average DM overdensity Δ_c of 200. For an isothermal singular sphere, the virial temperature

$$T_{\text{vir}} = \frac{\mu m_p V_c^2}{2k}, \quad (1)$$

where $V_c^2 = GM/r_{200}$ is the circular velocity (see Bryan & Norman 1998, with $\beta = 1$). Here μ is the mean molecular weight in units of the proton mass m_p , and k

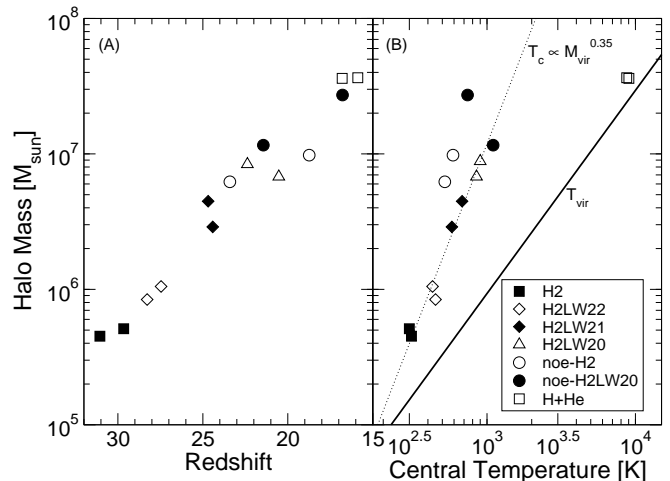


FIG. 3.— *Panel A:* Halo masses of the most massive halos as function of redshift when they reach a central overdensity of 10^7 . This allows to translate the mass values in Panel B to be converted to cooling redshifts. It marks the runs with H+He (filled squares), H_2 (open squares), $F_{LW} = 10^{-22}$ (open diamonds), $F_{LW} = 10^{-21}$ (filled diamonds), no residual electrons (open circles), and extreme feedback noe-LW20 (filled circles) runs. The two data points for each symbol represent simulations A and B. Even for the most extreme cases of feedback cooling occurs much earlier than in the atomic line cooling only case. *Panel B:* Central temperatures of most massive halo in the simulation as a function of its mass at different redshifts. The virial temperature computed from the dark matter halo mass at redshift 20 is the solid line. The dotted line is the fitted relationship between the central gas temperatures and the halo mass in models with residual electrons and H_2 cooling.

is Boltzmann’s constant. We use this definition of T_{vir} in this paper with $\mu = 0.59$. We choose this value of μ to be consistent with the literature on galaxy formation even though the halos presented in this paper are neutral and have $\mu = 1.22$.

3. RESULTS

We first describe the halo properties at collapse. Then we compare them to previous studies of collapsing halos in the presence of a soft UVB.

3.1. Halo Properties

Figure 2 shows density-squared weighted projections of gas density and temperature when each calculation can cool and collapse to an overdensity of 10^7 . It illustrates the large difference in the sizes and morphologies of the collapsing halos in the various cases of negative feedback. All panels have the same field of view of 1.2 proper kpc and same color scales. It is clear from the relative sizes of the collapsing halos that the critical halo mass to cool increases with the amount of negative feedback. The virial shock and numerous central shocks heat the gas to the virial temperature. The central shocks create fine structure seen in the temperature projections. In all of the H_2 cases, we see neither fragmentation nor large-scale disk formation. The internal structures of the halos with H_2 cooling and residual free electrons are similar to previous studies of Pop III star forming halos (MBA01; Abel et al. 2000, 2002; Bromm et al. 2002; Yoshida et al. 2003), exhibiting a turbulent medium with a radially monotonically decreasing density profile and a cool central core.

Figure 3A depicts the halo mass and redshift when the halo collapses for all of the runs, and Figure 3B shows their central temperature at the same epoch. The collapse redshifts, z_a and z_b , are also listed in Table 1 for simulations A and B, respectively. As seen in other studies (MBA01, YAHS03), the minimum DM halo mass to collapse increases with the background intensity. The H+He case predictably collapses at $T_{\text{vir}} \sim 10^4$ K, and all of the halos with H₂ cooling collapse at much smaller masses. The temperature of the central core increases with halo mass from 300 K to 1000 K for halo masses $4 \times 10^5 M_\odot$ and $10^7 M_\odot$. Restricting the data to models with residual electrons, the central temperature increases as a power-law,

$$T_c = AM_{\text{vir}}^B, \quad (2)$$

where $A = 3.1_{-0.9}^{+1.3}$, $B = 0.355 \pm 0.024$, and M_{vir} is in units of solar masses. This relationship is plotted in Figure 3.

With neither residual electrons nor an UVB (noe-H2), the most massive halo collapses at $9.8 (6.2) \times 10^6 M_\odot$ at $z = 18.7 (23.4)$. Here H₂ formation in the gas phase can only become important when sufficient free electrons are created by collisional ionization. Virial heating in the center of halos can increase temperatures up to twice the virial temperature (Wise & Abel 2007) that collisionally ionizes hydrogen in the central shocks and initiates H₂ cooling (Shapiro & Kang 1987) in halos well below virial temperatures of 10^4 K. These shocks are abundant throughout the central regions. Figure 4 shows radial profiles of temperature and electron fraction for both simulations and depicts gas shock-heating up to 2×10^4 K and raising electron fractions up to 10^{-3} . The electron fractions remain at unrealistically low values less than 10^{-6} in low density regions where gas has not been collisionally ionized. The higher density regions have condensed to densities above $3 \times 10^2 \text{ cm}^{-3}$ after free electrons in protogalactic shocks induced H₂ cooling.

A similar but extreme model, noe-H2LW20, demonstrates that even in the presence of a very large UVB of $F_{\text{LW}} = 10^{-20}$ gas is able to form a cool and dense central molecular core at a mass of $2.7 (1.1) \times 10^7 M_\odot$ at redshift 16.8 (21.4). Two major mergers in simulation A occur between $z = 17$ –21, and the associated heating allows the halo to begin cooling by H₂. A central core only forms once the system is adequately relaxed after the mergers, which causes the collapse mass difference between the realizations.

By not fully resolving weak shocks in our main calculations, it is possible to underestimate the electron fraction. We performed SimB-H2LW20 with an additional refinement criterion that resolves the “cooling length”, $l_{\text{cool}} = t_{\text{cool}}/c_s$, by at least 2 cells. The large- and small-scale structure in the simulation is unchanged. When we resolve these weak shocks, the increased electron fraction marginally accelerates the collapse, which occurs 780 kyr earlier at $z = 22.5$. The virial mass at this time is $8.0 \times 10^6 M_\odot$ compared with $8.4 \times 10^6 M_\odot$. Hence we believe that the critical halo mass to collapse as a function of the LW background is independent of this refinement criterion.

The combination of a recent major merger and collisional ionization produces complex structures as seen in the density and temperature projections of the SimA-

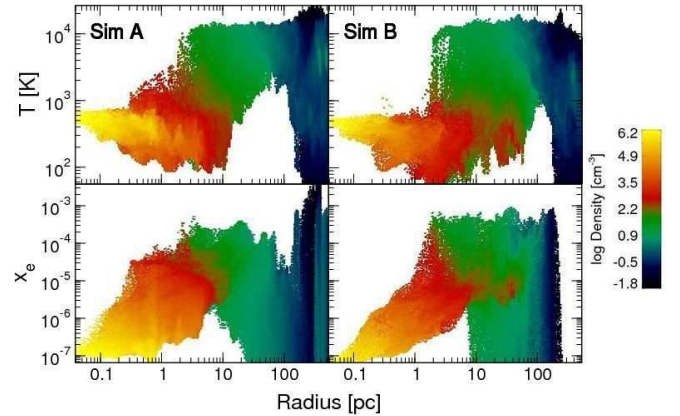


FIG. 4.— Radial profiles of temperature (*top*) and electron fraction (*bottom*) colored by density for the “noe-” simulations with no residual free electrons or UVB in simulation A (*left*) and B (*right*). The virial temperatures of these halos are 4600K and 4200K for simulation A and B, using equation (1) with $\mu = 0.59$.

Noe-LW20 and SimB-Noe- calculations in Figure 2, unlike the other H2 models with a single cool central core.

3.2. Comparison to Previous Studies

Through a series of AMR calculations with varying UVB intensities, MBA01 found the minimum DM halo mass

$$M_{\text{crit}} = 2.5 \times 10^5 + 1.7 \times 10^6 (F_{\text{LW}}/10^{-21})^{0.47} M_\odot \quad (3)$$

in order to cool and condense 4% of the baryons. This fraction of cool and dense gas agrees with simulations of the formation of Pop III stars (Abel et al. 2002; Yoshida et al. 2006). There is some scatter of ~ 0.5 dex in this threshold mass (see also YAHS03). For the UVB intensities used in our models ($F_{\text{LW}} = 0, 10^{-22}, 10^{-21}, 10^{-20}$), the critical collapse masses are $2.5 \times 10^5, 8.4 \times 10^5, 2.0 \times 10^6$, and $5.4 \times 10^6 M_\odot$. Our calculations with H₂ cooling and residual free electrons agree with the results of MBA01.

YAHS03 studied the minimum collapse mass but also included the effects of self-shielding. Through their SPH simulations and arguments using equilibrium H₂ abundances, they conclude that an UVB intensity of $J_{21} = 0.1$ nearly prevents halo collapses below $T_{\text{vir}} \simeq 7000$ K where Ly α cooling becomes efficient. They also deduce that $J_{21} = 1.0$ completely prevents any H₂ cooling in these low-mass halos, based on H₂ dissociation timescales. We find the contrary in our H2LW21 and H2LW20 calculations where the most massive halo collapses with a mass of $4.5 (2.9) \times 10^6 M_\odot$ and $8.4 (6.8) \times 10^6 M_\odot$, respectively. Even in our noe- runs, the halo collapses when $T_{\text{vir}} \sim 4000$ K, i.e. before Ly α cooling becomes important, which is around the same mass scale that the H2LW20 runs condense. We ignore self-shielding in our calculations, but this would only decrease the critical collapse mass and strengthens our main conclusion that H₂ cooling is always dominant, even in the presence of a large LW flux.

YAHS03 used cosmological SPH simulations and H₂ formation and dissociation timescales to argue that a LW background intensity of $J_{21}^{\text{LW}} > 0.1$ suppresses H₂ formation so halos cannot cool before virial temperatures of

7000 K are reached. Employing the same argument, we see that the H_2 formation timescale

$$t_{\text{H}_2} = \frac{n_{\text{H}_2}}{k_{\text{H}-} n_{\text{H}} n_{\text{e}}} = \frac{f_{\text{H}_2}}{0.92 k_{\text{H}-} f_{\text{e}} n} \approx 30 \text{ kyr}, \quad (4)$$

with typical central values found in high-redshift halos before any radiative cooling becomes efficient (see Wise & Abel 2007). Here $f_{\text{H}_2} = 10^{-6}$ and $f_{\text{e}} = 10^{-4}$ are the H_2 and electron number fraction, respectively, and $n = 10 \text{ cm}^{-3}$ is the baryon number density. $k_{\text{H}-} \approx 10^{-15} \text{ cm}^3 \text{ s}^{-1}$ is the H^- formation rate coefficient by electron photo-attachment at $T = 1000 \text{ K}$ (Abel et al. 1997). This timescale is a factor of 1000 smaller than the value calculated in YAHS03 because we use the quantities from the halo center as compared to the mean values. The H_2 dissociation timescale is $k_{\text{diss}}^{-1} = 23/J_{21} \text{ kyr}$, which is comparable with t_{H_2} using the values above.

The halo characteristics and the collapse redshift will likely depend on halo merger histories as seen in these two realizations. The better statistics of MBA01 sampled this effect well. Here the scatter of threshold mass is ~ 0.5 dex and is smaller than the mass difference between halos with virial temperatures of 4000K and 10000K. Thus our limited sample of halos should not change our result of the importance of H_2 cooling in halos well below $T_{\text{vir}} = 10^4 \text{ K}$, even with very large LW radiation backgrounds.

4. DISCUSSION

Structure formation in the high-redshift universe is contained within shallow potential wells that are sensitive to negative feedback from a UVB. Additionally local positive and negative feedback will influence star formation and further complicate estimates of halo mass scales. Some examples include

- *Positive feedback*— Enhanced H_2 formation in relic H II regions (e.g. Ferrara 1998; O’Shea et al. 2005; Johnson et al. 2007) and ahead of the H II ionization front (Ricotti et al. 2001; Ahn & Shapiro 2007), dust and metal line cooling (Glover 2003; Schneider et al. 2006; Jappsen et al. 2007),
- *Negative feedback*— Baryonic expulsion from host halos (Whalen et al. 2004; Kitayama et al. 2004; Yoshida et al. 2007; Abel et al. 2007), photo-evaporation (Susa & Umemura 2006), entropy floors (Oh & Haiman 2003).

These processes are not within the scope of this paper and will be considered in later publications that utilize three-dimensional radiation hydrodynamic simulations with Pop III star formation. Here we only focused on the effects of a UVB on low-mass halos.

4.1. The Nature of the UVB

The intensity of the UVB is a monotonically increasing function of redshift as more halos form stars. The UVB increases on the order of a Hubble time, which is much shorter than a dynamical time of a collapsing halo and justifies the use of a constant intensity in our calculations.

Self-consistent studies that evolve the UVB according to star formation rates only find J_{21}^{LW} to be in the range of 0.01 and 0.1 at redshifts 15–20 (YAHS03, WA05). WA05

calibrated their model against the WMAP1 measurement of $\tau = 0.17$. With the WMAP3 result of the electron scattering optical depth $\tau = 0.09$ and less small-scale power, UVB intensities will be even lower at these redshifts.

We can relate reionization to LW radiation by equating J_{21} in the LW band to a common quantity in reionization models, the ratio of emitted hydrogen ionizing photons to baryons, $n_{\gamma, \text{HI}}/\bar{n}_b$, where $\bar{n}_b \simeq 2 \times 10^{-7}(1+z)^3 \text{ cm}^{-3}$ is the cosmic mean of the baryon number density. Assuming that J_{LW} is constant in the LW band, the number density of LW photons is

$$n_{\gamma, \text{LW}} = \frac{4\pi}{c} \int_{\nu_1}^{\nu_2} \frac{J_{\text{LW}}}{h_p \nu} d\nu = 1.19 \times 10^{-5} J_{21}^{\text{LW}} \text{ cm}^{-3}, \quad (5)$$

where h_p is Planck’s constant and $\nu_1, \nu_2 = 2.70 \times 10^{15} \text{ Hz}, 3.26 \times 10^{15} \text{ Hz}$ bound the LW band. To relate J_{21} to $n_{\gamma, \text{HI}}/\bar{n}_b$, we must consider the intrinsic ionizing spectrum and absorption from the IGM and host halo. At redshift 20, the majority of star forming halos host Pop III stars that emit a factor $\phi_{\text{HI}} \simeq 10$ more hydrogen ionizing photons than LW photons because of its $\sim 10^5 \text{ K}$ surface temperature. Since the number density of sources exponentially increases with redshift, the majority of the early UVB at a given redshift originates from cosmologically nearby ($\Delta z/z \sim 0.1$) sources. Lyman line resonances absorb a fraction $f_{\text{abs}} \sim 0.1$ of the LW radiation in the intergalactic medium in this redshift range, producing a sawtooth spectrum (Haiman et al. 1997). Additionally, absorption in the host halo reduces the number of ionizing photons that escape into the IGM by a fraction f_{esc} . For Pop III halos, this factor is close to unity (Yoshida et al. 2007; Abel et al. 2007). By considering these multiplicative processes, we now estimate

$$\begin{aligned} \frac{n_{\gamma, \text{HI}}}{\bar{n}_b} &= \frac{n_{\gamma, \text{LW}}}{\bar{n}_b} \left(\frac{1+z}{20} \right)^{-3} \phi_{\text{HI}} f_{\text{esc}} f_{\text{abs}}^{-1} \\ &= 0.64 J_{21} \left(\frac{1+z}{20} \right)^{-3} \left(\frac{\phi_{\text{HI}}}{10} \right) \left(\frac{f_{\text{esc}}}{1} \right) \\ &\quad \times \left(\frac{f_{\text{abs}}}{0.1} \right)^{-1} \end{aligned} \quad (6)$$

This estimate is in agreement with the reionization models of Haiman et al. (2000) and WA05 (see also Gnedin & Ostriker 1997). These models find that sources produce a large UVB of $J_{21} \sim 1$ prior to reionization. When Pop III stars dominate the UVB, the LW radiation will be small in comparison to the volume averaged hydrogen ionizing emissivity because of the intrinsically hard Pop III spectra that peaks at $\sim 300\text{\AA}$. Hence high-redshift halos should not be exposed to a large UVB, i.e. $J_{21} \gtrsim 0.1$, and H_2 formation will remain important before reionization.

Nearby star formation can boost the LW radiation over its background value, but these bursts are short-lived as Pop III lifetimes are only $\sim 3 \text{ Myr}$ (Schaerer 2002). For example, a $100 M_{\odot}$ star produces 10^{50} LW photons s^{-1} and will produce $J_{21}^{\text{LW}} > 0.1$ in the surrounding 3 proper kpc, neglecting any H_2 self-shielding.

The LW background is uniform outside these spheres of influence. The bursting nature of Pop III star formation does not affect the time evolution of the background.

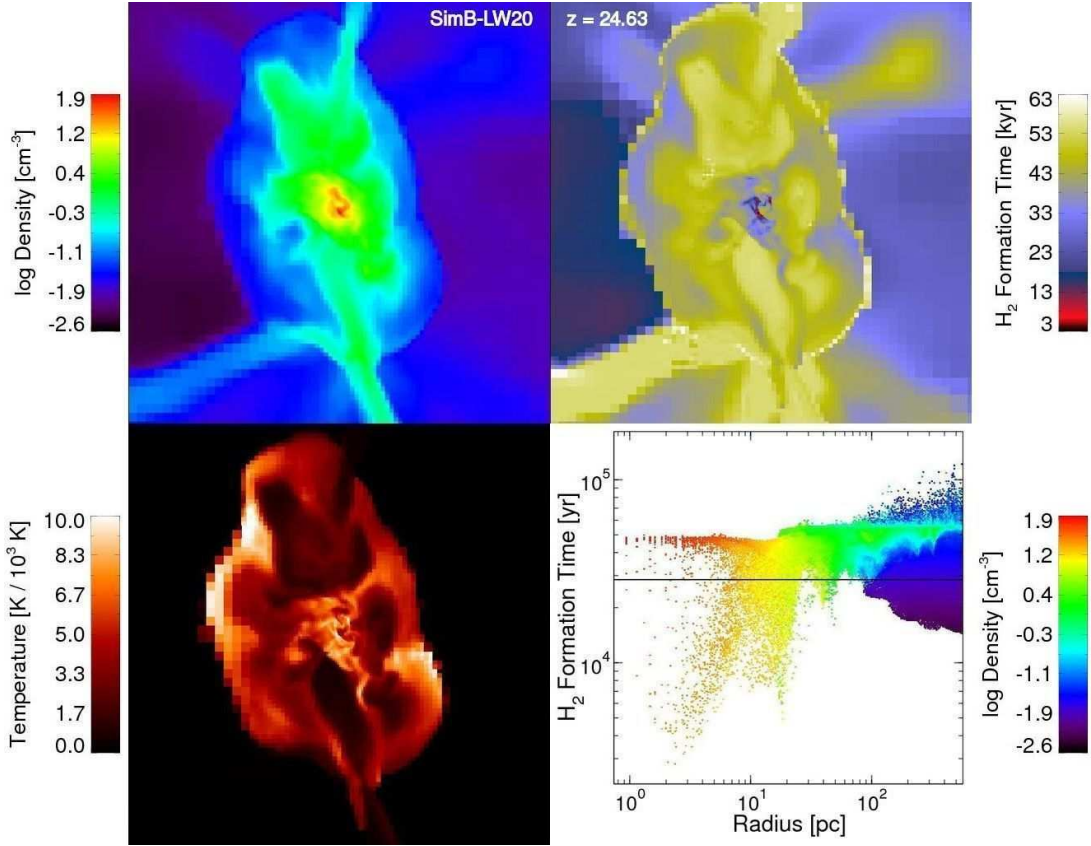


FIG. 5.— The most massive halo in SimB-LW20 ($F_{\text{LW}} = 10^{-20}$) twenty million years before the cooling core collapses. Slices of gas density (left) and the H_2 formation timescale (Eq. [4]; right) through the densest point in the halo are in the top row. The bottom row contains a slice of temperature (left) and a radial profile of the H_2 formation timescale, colored by gas density. The phase diagram and density slice have the same color scale. The slices have a field of view of 500 proper pc. In the central shocks, H_2 formation timescales are lower than the dissociation timescale of 28 kyr with $F_{\text{LW}} = 10^{-20}$ that is denoted by the horizontal line in the radial profile. The central core is now efficiently cooling and will collapse 20 Myr after these data.

The intensity only depends on the number of sources in a redshift range $\Delta z/z = 13.6 \text{ eV} / 11.18 \text{ eV} - 1$, where the two energies bound the LW band, because any radiation redward of the Lyman break contributes to the LW background. Using a conservative minimum halo mass for Pop III star forming halos of $3 \times 10^6 M_\odot$ at redshift 20, there are ~ 42000 halos that have hosted a Pop III star in the volume contained within Δz , using WMAP3 parameters with Sheth-Tormen formalism. Clearly the background is uniform considering the sheer number of sources within this optically thin volume. Local perturbations from Pop III star formation should only affect the timing of nearby star formation but not the global star formation rate.

4.2. H_2 Cooling within a UVB

Figure 5 shows SimB-LW20 twenty million years before the central core condenses. At this time, the core is just beginning to cool by H_2 , catalyzed by the free electrons created in the central shocks. In these shocks, temperatures reach $1.4 \times 10^4 \text{ K}$ and electron fractions up to 10^{-3} exist there. These conditions result in H_2 formation timescales less than 25 kyr, which is necessary to cool in a UVB of $J_{21} \sim 1$. Within the central 10 pc, hot and cold gas phases exist. The hot phase exists behind the shocks that have lower densities around 10 cm^{-3} and $t_{H_2} < 25 \text{ kyr}$. This is where H_2 cooling is catalyzed by

collisional ionization in these shocks. The cold phase has already cooled through H_2 and has high densities and larger t_{H_2} values. Both phases are apparent in the panels of Figure 5. Similar conditions create H_2 in the collapses in the “noe” calculations, which have sufficient gravitational potential energy, resulting in temperatures above 10^4 K in central shocks. Hence H_2 formation is possible in the centers of high-redshift halos with virial temperatures below 10^4 K , even with a UVB of intensity $J_{21}^{\text{LW}} \sim 1$, larger than expected from semi-analytic models of reionization.

4.3. Impact on Semi-analytic Models

Two consequences of a lower critical Ly α cooling halo mass are more frequent and earlier galaxy formation and higher mass fractions in cooling halos. At redshift 20, e.g., abundances of $T_{\text{vir}} = 4000 \text{ K}$ halos are an order of magnitude larger than $T_{\text{vir}} = 10^4 \text{ K}$ halos, resulting from the exponential nature of Press-Schechter formalism. The mass fraction contained in these halos is three times higher than 10^4 K halos. In semi-analytic models of reionization and chemical enrichment, the star formation rate (SFR) is linearly dependent on the collapsed mass fraction since the SFR is usually a product of mass fraction and star formation efficiency, which is the fraction of gas collapsing into stars (e.g. Haiman et al. 1997). The star formation efficiency for primordial stars

is $\sim 10^{-3}$ with a single massive star forming in dark matter halos with mass $\sim 10^6 M_\odot$ (Abel et al. 2002; Bromm et al. 2002; Yoshida et al. 2006). This fraction may rise to a few percent in dwarf galaxies as widespread star formation occurs (Taylor et al. 1999; Gnedin 2000; Walter et al. 2001). Various studies predict that a majority of the reionizing flux originates from dwarf galaxies (e.g. Cen 2003; Sokasian et al. 2004; Haiman & Bryan 2006). If the mass contained in star forming halos is three times greater than previously thought, some of the predicted attributes, e.g. photon escape fractions and star formation efficiencies, of high-redshift dwarf galaxy will require appropriate adjustments to match observations, such as the WMAP3 measurement of optical depth to electron scattering (Page et al. 2007) and Gunn-Peterson troughs at $z \sim 6$ (Becker et al. 2001; Fan et al. 2002).

5. SUMMARY

We conducted a suite of fourteen cosmology AMR simulations that focus on the importance of H_2 cooling with various degrees of negative feedback. We summarize the findings of each model below.

1. The calculations with a UVB of $F_{\text{LW}} = (0, 10^{-22}, 10^{-21})$ agree with the results of MBA01, where the critical collapse halo mass increases as a function of UVB intensity.

2. Above $F_{\text{LW}} = 10^{-21}$, it had been argued that an H_2 dissociating background would inhibit any H_2 formation until the halo could cool through $\text{Ly}\alpha$ cooling. We showed that central shocks provide sufficient free electrons from collisional ionization to drive H_2 formation faster than dissociation rates even in a $F_{\text{LW}} = 10^{-20}$ background.

3. In our “noe-” models, we explored when collisional ionization becomes important and conducive for H_2 formation. This occurs at $T_{\text{vir}} \sim 4000$ K. Recent major mergers above this mass scale create complex cooling structures, unlike the non-fragmented central cores in smaller halos.

4. Even our most extreme assumptions of $J_{21} = 1$ ($F_{\text{LW}} \simeq 10^{-20}$) and no residual free electrons cannot de-

feat the importance of H_2 cooling in the early universe.

O’Shea & Norman (2007) independently studied halo collapses with *Enzo* and similarly considered primordial gas chemistry and nine different UVB intensities ranging from zero to $J_{21} = 1$. They agree with our conclusions in that primordial gas in $T_{\text{vir}} < 10^4$ K halos can catastrophically cool and collapse even in models with $J_{21} \geq 0.1$. They attribute the collapse to the increased H_2 cooling rates at higher temperatures that is caused by greater dynamical heating in halos with $M_{\text{vir}} \gtrsim 10^7 M_\odot$. The cooling rate per molecule is 100 times larger at 2000 K than at 500 K, typical of Pop III star-forming halos without an UVB. Most likely, the combination of the elevated H_2 cooling rates and electron fractions from internal protogalactic shocks instigate the halo collapses in a strong UVB ($J_{21} \geq 0.1$).

In any case, H_2 cooling triggers collapses in halos with virial temperatures well below 10^4 K. The lower critical halo mass, corresponding to $T_{\text{vir}} \sim 4000$ K, increases mass fraction contained in these halos by three times at redshift 20 and the number density of high-redshift star forming halos by an order of magnitude! By considering additional cases of extremely large negative feedback, we have strengthened the results of MBA01 that H_2 cooling plays a key role in high-redshift structure formation. We conclude that a UVB only delays and never completely suppresses H_2 formation and cooling and subsequent star formation in these low-mass halos.

This work was supported by NSF CAREER award AST-0239709 from the National Science Foundation. We appreciate the helpful feedback, which enhanced the presentation of this paper, from the referee, Simon Glover. We thank Marcelo Alvarez, Greg Bryan, and Naoki Yoshida for providing constructive comments on an early draft. We are grateful for the continuous support from the computational team at SLAC. We performed these calculations on 16 processors of a SGI Altix 3700 Bx2 at KIPAC at Stanford University.

REFERENCES

- Abel, T., Anninos, P., Zhang, Y., & Norman, M. L. 1997, *New Astronomy*, 2, 181
 Abel, T., Anninos, P., Norman, M. L., & Zhang, Y. 1998, *ApJ*, 508, 518
 Abel, T., Bryan, G. L., & Norman, M. L. 2000, *ApJ*, 540, 39
 Abel, T., Bryan, G. L., & Norman, M. L. 2002, *Science*, 295, 93
 Abel, T., Wise, J. H., & Bryan, G. L. 2007, *ApJ*, 659, L87
 Ahn, K., & Shapiro, P. R. 2007, *MNRAS*, 375, 881
 Alvarez, M. A., Shapiro, P. R., Ahn, K., & Iliev, I. T. 2006, *ApJ*, 644, L101
 Anninos, P., Zhang, Y., Abel, T., & Norman, M. L. 1997, *New Astronomy*, 2, 209
 Baugh, C. M., Benson, A. J., Cole, S., Frenk, C. S., & Lacey, C. 2003, *The Mass of Galaxies at Low and High Redshift*, 91
 Becker, R. H. et al. 2001, *AJ*, 122, 2850
 Bertschinger, E. 1995, *ArXiv Astrophysics e-prints*, arXiv:astro-ph/9506070
 Bertschinger, E. 2001, *ApJS*, 137, 1
 Bromm, V., Coppi, P. S., & Larson, R. B. 2002, *ApJ*, 564, 23
 Bromm, V. & Loeb, A. 2003, *ApJ*, 596, 34
 Bryan, G. L. & Norman, M. L. 1997, in *Computational Astrophysics*, eds. D. A. Clarke and M. Fall, ASP Conference #123
 Bryan, G. L., & Norman, M. L. 1998, *ApJ*, 495, 80
 Bryan, G. L. & Norman, M. L. 1999, in *Workshop on Structured Adaptive Mesh Refinement Grid Methods*, IMA Volumes in Mathematics No. 117, ed. N. Chrisochoides, p. 165
 Cen, R. 1992, *ApJS*, 78, 341
 Cen, R. 2003, *ApJ*, 591, L5
 Ciardi, B., & Ferrara, A. 2005, *Space Science Reviews*, 116, 625
 Couchman, H. M. P. 1991, *ApJ*, 368, L23
 Dekel, A., & Rees, M. J. 1987, *Nature*, 326, 455
 Draine, B. T., & Bertoldi, F. 1996, *ApJ*, 468, 269
 Fan, X., Narayanan, V. K., Strauss, M. A., White, R. L., Becker, R. H., Pentericci, L., & Rix, H. 2002, *AJ*, 123, 1247
 Ferrara, A. 1998, *ApJ*, 499, L17
 Galli, D., & Palla, F. 1998, *A&A*, 335, 403
 Glover, S. C. O. 2003, *ApJ*, 584, 331
 Glover, S. C. O., & Brand, P. W. J. L. 2001, *MNRAS*, 321, 385
 Gnedin, N. Y. 2000, *ApJ*, 535, L75
 Gnedin, N. Y., & Abel, T. 2001, *New Astronomy*, 6, 437
 Gnedin, N. Y., & Ostriker, J. P. 1997, *ApJ*, 486, 581
 Haiman, Z., Abel, T., & Rees, M. J. 2000, *ApJ*, 534, 11
 Haiman, Z., & Bryan, G. L. 2006, *ApJ*, 650, 7
 Haiman, Z., & Loeb, A. 1997, *ApJ*, 483, 21
 Haiman, Z., Rees, M. J., & Loeb, A. 1997, *ApJ*, 476, 458
 Haiman, Z., Thoul, A. A., & Loeb, A. 1996, *ApJ*, 464, 523
 Jappsen, A.-K., Glover, S. C. O., Klessen, R. S., & Mac Low, M.-M. 2007, *ApJ*, 660, 1332
 Johnson, J. L., Greif, T. H., & Bromm, V. 2007, *ApJ*, 665, 85
 Katz, N., Weinberg, D. H., & Hernquist, L. 1996, *ApJS*, 105, 19
 Kitayama, T., Yoshida, N., Susa, H., & Umemura, M. 2004, *ApJ*, 613, 631

- Machacek, M. E., Bryan, G. L., & Abel, T. 2001, *ApJ*, 548, 509 (MBA01)
- Martin, P. G., Schwartz, D. H., & Mandy, M. E. 1996, *ApJ*, 461, 265
- Mesinger, A., Bryan, G. L., & Haiman, Z. 2006, *ApJ*, 648, 835
- O’Shea, B. W., Abel, T., Whalen, D., & Norman, M. L. 2005, *ApJ*, 628, L5
- O’Shea, B. W. & Norman, M. L. 2007, *ApJ*, *submitted*, [arXiv:0706.4416](#)
- Oh, S. P., & Haiman, Z. 2002, *ApJ*, 569, 558
- Oh, S. P., & Haiman, Z. 2003, *MNRAS*, 346, 456
- Page, L., et al. 2007, *ApJS*, 170, 335
- Peebles, P. J. E. 1968, *ApJ*, 153, 1
- Peebles, P. J. E., & Dicke, R. H. 1968, *ApJ*, 154, 891
- Press, W. H. & Schechter, P. 1974, *ApJ*, 187, 425
- Rees, M. J., & Ostriker, J. P. 1977, *MNRAS*, 179, 541
- Ricotti, M., Gnedin, N. Y., & Shull, J. M. 2001, *ApJ*, 560, 580
- Ricotti, M., Gnedin, N. Y., & Shull, J. M. 2002b, *ApJ*, 575, 33
- Ricotti, M., Gnedin, N. Y., & Shull, J. M. 2002a, *ApJ*, 575, 49
- Saslaw, W. C., & Zipoy, D. 1967, *Nature*, 216, 976
- Schaerer, D. 2002, *A&A*, 382, 28
- Schneider, R., Omukai, K., Inoue, A. K., & Ferrara, A. 2006, *MNRAS*, 369, 1437
- Shapiro, P. R., & Kang, H. 1987, *ApJ*, 318, 32
- Shapiro, P. R., Giroux, M. L., & Babul, A. 1994, *ApJ*, 427, 25
- Sheth, R. K. & Tormen, G. 2002, *MNRAS*, 329, 61
- Sokasian, A., Yoshida, N., Abel, T., Hernquist, L., & Springel, V. 2004, *MNRAS*, 350, 47
- Spergel, D. N., et al. 2003, *ApJS*, 148, 175
- Spergel, D. N., et al. 2007, *ApJS*, 170, 377
- Susa, H., & Umemura, M. 2006, *ApJ*, 645, L93
- Taylor, C. L., Hüttemeister, S., Klein, U., & Greve, A. 1999, *A&A*, 349, 424
- Tegmark, M., Silk, J., Rees, M. J., Blanchard, A., Abel, T., & Palla, F. 1997, *ApJ*, 474, 1
- Walter, F., Taylor, C. L., Hüttemeister, S., Scoville, N., & McIntyre, V. 2001, *AJ*, 121, 727
- Whalen, D., Abel, T., & Norman, M. L. 2004, *ApJ*, 610, 14
- White, S. D. M., & Frenk, C. S. 1991, *ApJ*, 379, 52
- White, S. D. M., & Rees, M. J. 1978, *MNRAS*, 183, 341
- Wise, J. H., & Abel, T. 2005, *ApJ*, 629, 615 (WA05)
- Wise, J. H., & Abel, T. 2007, *ApJ*, 665, 899
- Yoneyama, T. 1972, *PASJ*, 24, 87
- Yoshida, N., Abel, T., Hernquist, L., & Sugiyama, N. 2003, *ApJ*, 592, 645 (YAHS03)
- Yoshida, N., Oh, S. P., Kitayama, T., & Hernquist, L. 2007, *ApJ*, 663, 687
- Yoshida, N., Omukai, K., Hernquist, L., & Abel, T. 2006, *ApJ*, 652, 6
- Zhang, Y., Anninos, P., & Norman, M. L. 1995, *ApJ*, 453, L57